Available online at www.sciencedirect.com
SCIENCE DIRECT®
Metabolic Engineering 7 (2005) 88–103
METABOLIC ENGINEERING
www.elsevier.com/locate/ymben

Evolution of intrahepatic carbon, nitrogen, and energy metabolism in a D-galactosamine-induced rat liver failure model

Tadaaki Yokoyama, Scott Banta, François Berthiaume, Deepak Nagrath, Ronald G. Tompkins, Martin L. Yarmush*

Center for Engineering in Medicine/Surgical Services, Massachusetts General Hospital, Harvard Medical School and Shriners Hospital for Children, 51 Blossom Street, Boston, MA 02114, USA

Received 14 July 2004; received in revised form 10 September 2004; accepted 20 September 2004
Available online 13 November 2004

Abstract

A clearer picture of the hepatic metabolic pathways affected by fulminant hepatic failure (FHF) would help develop nutritional support and nonsurgical therapies for FHF. We characterized the evolution of hepatic metabolism in a rat model of FHF using an isolated perfused liver system together with a mass-balance model of intermediary metabolism. Principal component analysis (PCA) was used to identify potential new sensitive markers for FHF. To induce FHF, rats were given two D-galactosamine injections under fasting conditions. Controls were fasted only. Livers were harvested 1, 4, 8, and 12 h later and perfused with Eagle minimal essential medium supplemented with amino acids and bovine serum albumin, and equilibrated with 95% O_2/5% CO_2. At the 1 h time point, lactate release increased concomitant with a decrease in gluconeogenesis, TCA cycle and mitochondrial electron transport fluxes. At 4 h, amino acid metabolism and urea cycle fluxes were significantly depressed. By 8 h, gluconeogenesis had switched to glycolysis. By 12 h, amino acid metabolism was broadly inhibited, and there was a net release of many amino acids. Mass-balance analysis shows that the main source of ATP production in the FHF liver gradually changed from mitochondrial oxidative phosphorylation to glycolysis. PCA suggests that a linear combination of glucose, lactate, and glutamine concentrations in arterial plasma is a sensitive marker for FHF. We conclude that D-galactosamine causes early mitochondrial dysfunction while glycolytic ATP synthesis remains functional. Markers that are indirectly linked to these pathways may be used to evaluate the progression of FHF.

Keywords: Perfused liver; Metabolic flux analysis; Principal component analysis; Mitochondria; Amino acids

1. Introduction

Orthotopic liver transplantation is the most widely accepted treatment for fulminant hepatic failure (FHF) (Ascher et al., 1993; Bismuth et al., 1987; Devictor et al., 1992; Lee, 1993), however, the continuous shortage of donors and side effects of long-term immunosuppression motivate the search for cheaper and less invasive alternatives. Although the precise pathogenesis of hepatic encephalopathy, the main cause of death in FHF, is not precisely known, a considerable body of evidence suggests that it is linked to a failure of hepatic clearance of gut-derived substances (e.g., ammonia, γ-aminobutyric acid) as well as altered amino acid metabolism that results in changes in neurotransmitters. In the latter category, phenylalanine and tyrosine-derived monoamines (e.g., phenylethylamine, tyramine, phenylethanolamine, octopamine) (Ozawa et al., 1992, 1983; Saibara et al., 1991), as well as tryptophan-derived monoamines (e.g., serotonin [5-hydroxytryptamine] and tryptamine) (Clemmesen et al., 2000; Roth et al., 1994), have been studied extensively. To counteract the observed shifts in metabolite levels in the systemic circulation, solutions rich in branched chain amino acids [(BCAA) leucine, isoleucine, and valine] have been used

*Corresponding author.
E-mail address: fberthia@sbi.org (M.L. Yarmush).

1096-7176/$ - see front matter © 2004 Elsevier Inc. All rights reserved.
doi:10.1016/j.ymben.2004.09.003

as nutritional supplements (Fischer et al., 1976; Mizock, 1999). These formulas were often found to be beneficial, although some studies failed to demonstrate positive effects (Mizock, 1999).

Systemic changes in metabolite levels do not solely reflect alterations in liver function, but also changes in the metabolism of a number of other tissues that are also affected during FHF. A clearer picture of which pathways are affected specifically in the liver could provide a more rational basis for the development of nutritional support and other non-surgical medical therapies. In order to characterize the metabolic state of the liver in the absence of systemic effects, isolated perfused liver systems can be used to study a wide range of metabolic conditions (Arai et al., 2001; Yamaguchi et al., 1997). Furthermore, steady-state mass balance models can be used to derive intrahepatic metabolic fluxes by Metabolic Flux Analysis (MFA), thus providing a comprehensive map of the metabolic state of the organ (Arai et al., 2001; Lee et al., 2000).

In a prior study, we characterized the metabolic state of liver 12 h after D-galactosamine-induced FHF in fasted rats. We found significantly decreased hepatic gluconeogenesis, which correlated with a reduction in amino acid entry into various points of the tricarboxylic acid (TCA) cycle (Arai et al., 2001). Furthermore, FHF inhibited intrahepatic aspartate synthesis, which resulted in a 50% reduction in urea cycle flux, and ammonia removal was quantitatively maintained by glutamine synthesis from glutamate and a decrease in the conversion of glutamate to α-ketoglutarate (Arai et al., 2001). Here, we characterized the evolution of alterations in intrahepatic metabolic fluxes over time in this rat model of FHF. We found that following D-galactosamine-induced FHF, the earliest metabolic perturbations detected include an inhibition of TCA cycle fluxes and some parts of the gluconeogenic pathway, with a significant increase in lactate release. Furthermore, the main source of ATP production in the FHF liver gradually changed from mitochondrial oxidative phosphorylation to glycolysis.

2. Materials and methods

2.1. Animals

Animal studies were carried out in accordance with National Research Council guidelines and approved by the Subcommittee on Research Animal Care and Laboratory Animal Resources of the Massachusetts General Hospital. Male Sprague-Dawley rats (Charles River Laboratories, Boston, MA) weighing 150–200 g were housed at 25 °C in a 12 h light-dark cycle and provided water and standard rat chow ad libitum. They were randomly divided into D-galactosamine-induced FHF and normal control groups.

2.2. Induction of fulminant hepatic failure in rat

D-galactosamine (Sigma Chemical Co., St. Louis, MO) was dissolved in saline and the pH adjusted to 7.0 with 1 N NaOH immediately prior to use. Rats were fasted for 12 h and administered 1.4 g/kg D-galactosamine intraperitoneally under light halothane anesthesia. While fasting continued, a second identical D-galactosamine injection was administered 12 h later. Animals were fasted for another 1, 4, 8, or 12 h, at which time perfusion was initiated. Control rats were fasted for 25, 28, 32, or 36 h and did not receive any other treatments before perfusion.

2.3. Isolated perfused rat liver studies

Isolated rat liver perfusions were performed according to a modification of Mortimore's methods (Mortimore and Surmacz, 1984) as described elsewhere (Arai et al., 2001). The liver was perfused via the portal vein at a constant flow rate of 15.0 ± 2.2 ml/g dry liver/min in a recirculating mode with Eagle's Minimum Essential Medium (Sigma) supplemented with 3% w/v bovine serum albumin (Fraction V; Sigma) and several amino acids so that the concentrations of individual amino acids in the perfusate were approximately twice those in postabsorptive rat plasma (Arai et al., 2001). Although no ammonia was added to the perfusate, it contained a basal initial level (69 ± 31 μM in control and 45 ± 41 μM in FHF groups; not statistically different) that most likely originated from partial glutamine degradation. The perfusate was gassed with humidified 95%O_2/5%CO_2 and maintained at 37 °C. Perfusate samples (1.5 ml each) were collected every 10 min for 60 min and stored at −80 °C. After 10 and 50 min, inflow and outflow perfusate samples were analyzed for O_2 and CO_2 with a 238 Blood Gas Analyzer (Chiron Diagnostics Co., Pittsburgh, PA). At the end of the perfusion, the whole liver was weighed, freeze-dried, and weighed again to determine the dry/wet weight ratio.

2.4. Assessment of liver injury

Blood was sampled from the abdominal aorta prior to initiating liver perfusion. Plasma levels of aspartate aminotransferase (AST) and alanine aminotransferase (ALT) were determined using commercially available kits (Sigma kits nos. 58 and 59) as parameters of liver injury.

2.5. Metabolite assays

Glucose and lactate concentrations in the perfusate/plasma samples were determined using commercial

assay kits (Sigma kits nos. 315 and 735). Urea content was measured by reacting with diacetyl monoxime using a commercial assay kit (Sigma kit no. 535-A). Acetoacetate (ACAC) and β-hydroxybutyrate (BHBA) concentrations were assayed enzymatically via nicotinamide adenine dinucleotide (NADH)-coupled reactions catalyzed by BHBA dehydrogenase (Zupke et al., 1998).

2.6. Amino acid analysis

Amino acids and ammonia in the perfusate/plasma were quantified by high-performance liquid chromatography on a Waters 2690 Separations Module and 474 Scanning Fluorescence Detector (Waters Co., Milford, MA) set at excitation/emission wavelengths of 250/395 nm. Separation was carried out using a modification of Cohen's procedures (Cohen and De Antonis, 1994) adapted for a four eluent system of buffers (Arai et al., 2001). Samples were deproteinated by mixing 1:1 with acetonitrile, and derivatized with the Waters AccQ-Fluor Reagent Kit.

2.7. Calculation of rates of consumption or production of metabolites

Oxygen consumption and CO_2 generation rates were calculated by multiplying the perfusate flow rate by the outflow–inflow difference in the concentration of each species. In the above calculations, the increase in dissolved CO_2 concentration (pCO_2) was assumed to reflect total CO_2 production by the liver because the pH variation across the liver was too small to accurately assess the contribution of the HCO_3^- ion. The net consumption or release of the other extracellular metabolites was evaluated by linear regression of concentration vs. time data, correcting for perfusate volume changes due to sampling. All values were calculated and normalized to the dry weight of each perfused liver. The normalized values were then averaged for each experimental group, and expressed as means ± SE.

2.8. Metabolic flux determination by steady-state metabolic flux analysis

Two MFA models of liver were formulated, one corresponding to a gluconeogenic state (I) and the other to a glycolytic state (II). The pathways included in both models are: (a) TCA cycle, (b) urea cycle, (c) β-oxidation, (d) amino acid oxidation, (e) ketone body synthesis, and (f) the pentose phosphate pathway (PPP). In addition, gluconeogenesis reactions were added to model I, whereas glycolysis reactions were included in model II. The following pathways are typically inhibited by fasting and therefore not included in either model: (a) glycogen synthesis, (b) fatty acid synthesis, and (c) irreversible, energy requiring steps for de novo amino acid biosynthesis. The Appendix lists all reactions and relevant enzymes in both models. In model I, fluxes through pyruvate kinase (flux no. 8) and pyruvate dehydrogenase (flux no. 10) were set to zero. In model II, the flux through pyruvate carboxylase (flux no. 9) was set to zero. These constraints were necessary to avoid a futile cycle leading to a mathematical singularity in the network. Furthermore, in both models, the glucose 6-phosphate dehydrogenase flux (flux no. 59), an irreversible step, was required to be positive or zero. Measured rates of consumption/production were fitted to the two MFA models assuming pseudo steady-state as described elsewhere (Arai et al., 2001; Zupke and Stephanopoulos, 1995) and a "consistency index" for each fit was calculated to provide a quantitative measure of agreement between data and model. The MFA as well as PCA (described below) were performed using the MATLAB^{RN} software (Mathworks, Inc., Natick, MA). Fluxes for each liver were calculated and averages determined in each experimental group.

2.9. Principal component analysis

Principal component analysis (PCA) was used to identify parameters that differentiate between the control and FHF groups. Three analyses were carried out: (1) using measured arterial metabolite levels only, (2) using measured rates of uptake and release of metabolites during liver perfusions, and (3) using calculated intrahepatic fluxes. The measured and calculated data were scaled using mean centering. In each case, the analysis provides the relative weights for each data input as well as the proportion of the total variance in the data explained by each principal component (Skoal and Rohlf, 1969). For simplicity, only the fluxes with the five highest weights were kept.

2.10. Statistical analysis

Comparisons of measured metabolic rates and calculated fluxes between sham controls and time-matched FHF animals were made using unpaired Student's t-test. $P < 0.05$ was considered statistically significant.

3. Results

3.1. Changes in systemic levels of metabolites induced by D-galactosamine

Liver failure was induced by two D-galactosamine injections 12 h apart in fasted rats. This model boasts an 83% mortality rate at 7 days and was preferred over a nonlethal single D-galactosamine injection model (Shito et al., 2001). During the course of the study, which was

limited to 12 h following the second D-galactosamine injection, none of the rats died. Metabolic parameters indicative of FHF include decreased blood glucose levels (Lee, 1993) as well as increased levels of lactate (Bihari et al., 1985; Record et al., 1975; Saibara et al., 1994) and aromatic and many other amino acids (Record et al., 1976; Rosen et al., 1977; Zimmermann et al., 1989). Therefore, we first assessed the severity of hepatitis by measuring arterial plasma levels of these metabolites (Table 1). AST and ALT were 5–7 times controls 1 and 4 h after FHF induction, and then suddenly increased to 25–40 times controls at 8 and 12 h. Glucose levels were decreased and lactate levels increased in FHF throughout the experiment. Ammonia levels were significantly increased beginning 4 h after FHF induction, reaching levels 50–100% above controls. The amino acid profile was significantly altered at 4 and 12 h, with a transient recovery at 8 h. At 12 h, when the most dramatic changes were observed, almost all amino acids were elevated in FHF, except for arginine, which was decreased. The molar ratio of branched chain amino acids (BCAA) to aromatic amino acids (AAA), also known as the "Fischer ratio", was unchanged in FHF, except at the 12 h time point, when it was significantly decreased. The arterial ketone body ratio (AKBR) has been reported to reflect the mitochondrial redox potential, a measure of mitochondrial energy charge in liver (Ozawa et al., 1992, 1983; Skoal and Rohlf, 1969). The AKBR in FHF rats was 50% of control at the 1 h time point, returned to control levels at 4 and 8 h, and

Table 1
Effect of FHF on metabolite profile in arterial plasma[a]

	1 h		4 h		8 h		12 h	
	Ctrl ($n=6$)	FHF ($n=5$)	Ctrl ($n=9$)	FHF ($n=9$)	Ctrl ($n=11$)	FHF ($n=7$)	Ctrl ($n=6$)	FHF ($n=5$)
AST (U/L)	92±5	636±157**	96±3	510±100**	101±4	1151±378**	108±4	2750±573**
ALT (U/L)	40±4	319±66**	38±2	285±55**	34±3	685±232**	34±3	1331±111**
Glucose (g/L)	1.45±0.1	0.90±0.06*	1.64±0.15	1.13±0.06*	1.60±0.12	1.08±0.08*	2.04±0.06	1.24±0.04*
Lactate (mmol/L)	1.83±0.1	2.96±0.38**	1.81±0.08	2.36±0.23*	1.33±0.11	2.10±0.16**	1.62±0.19	3.58±0.08**
Ammonia (μmol/L)	35±4	49±8	44±2	63±6**	29±3	47±5**	36±2	73±7**
ACAC (mmol/L)	0.19±0.03	0.08±0.01*	0.20±0.02	0.10±0.01**	0.15±0.02	0.13±0.01	0.15±0.02	0.03±0.01**
BHBA (mmol/L)	1.09±0.23	0.81±0.05	0.82±0.10	0.72±0.09	0.87±0.12	0.69±0.11	0.78±0.14	0.87±0.07
AKBR	0.20±0.03	0.10±0.01*	0.25±0.02	0.16±0.02	0.19±0.02	0.22±0.04	0.21±0.04	0.03±0.01**
Aspartate (Asp)	3±1	3±1	3±1	2±1	1±0	4±1**	1±0	8±1**
Glutamate (Glu)	37±7	20±4	33±3	36±3	23±3	27±3	20±3	44±7**
Serine (Ser)	114±18	98±18	120±6	127±7	104±4	116±7	118±5	166±22
Asparagine (Asn)	36±7	65±14	35±3	44±3	26±3	29±3	27±2	53±8**
Glycine (Gly)	188±35	116±19	171±12	180±11	135±9	146±14	157±10	246±31*
Glutamine (Gln)	506±86	557±12	627±55	1015±51**	644±74	939±129	631±60	1411±152**
Histidine (His)	36±7	38±10	38±3	83±5**	30±2	67±6**	34±2	81±13**
Threonine (Thr)	154±22	96±21	173±13	166±13	123±14	131±10	144±14	137±30
Arginine (Arg)	69±11	17±6**	77±6	45±9**	59±5	29±6**	58±4	24±12**
Alanine (Ala)	180±39	163±46	191±14	180±16	154±10	151±14	149±6	294±39**
Proline (Pro)	95±23	95±19	118±8	116±7	89±5	100±6	80±2	138±14**
Tyrosine (Tyr)	50±6	57±18	55±5	77±7*	38±5	47±6	43±3	101±16**
Cysteine (Cys)	7±1	10±4	8±1	11±1	8±1	17±5	7±1	14±2*
Valine (Val)	79±11	67±13	96±6	119±8*	70±9	92±9	73±7	136±16**
Methionine (Met)	23±4	29±7	21±3	53±6**	17±1	35±4**	21±2	59±8**
Isoleucine (Ile)	41±5	36±6	52±3	59±4	38±4	40±3	52±4	52±6
Ornithine (Orn)	15±2	19±6	19±1	44±5**	15±3	33±3**	12±2	62±13**
Leucine (Leu)	51±6	60±12	69±5	92±6**	54±5	69±5	65±5	124±13**
Lysine (Lys)	160±29	56±13*	140±9	103±14*	133±12	98±19	114±9	131±23
Phenylalanine (Phe)	69±11	33±8*	67±5	98±8**	35±6	47±7	34±4	61±5**
Total amino acids	1905±289	1634±292	2115±111	2644±66**	1796±155	2215±166	1838±78	3345±271**
Gluconeogenic amino acids[b]	1840±281	1555±256	2027±107	2508±59**	1727±149	2113±165	1762±74	3160±256**
BCAA (Val+Leu+Ile)	172±22	162±31	216±14	270±14*	162±18	202±13	189±9	311±29**
AAA (Tyr+Phe)	111±16	90±25	122±8	175±10**	73±9	94±9	77±6	166±18**
BCAA/AAA	1.7±0.3	2.5±0.8	1.8±0.1	1.6±0.1	2.3±0.2	2.2±0.2	2.5±0.2	1.9±0.1**
Liver dry/wet ratio	0.24±0.006	0.23±0.002	0.23±0.007	0.24±0.005	0.24±0.005	0.25±0.007	0.24±0.005	0.23±0.005

*$P<0.05$ compared with control. **$P<0.01$ compared with control.

[a]Data are presented as mean±SE.

[b]Aspartate, asparagine, serine, glycine, glutamate, glutamine, histidine, threonine, alanine, proline, methionine, lysine, cysteine, tyrosine, phenylalanine, arginine, valine, and isoleucine.

decreased again to reach 10–25% control levels at 12 h. Overall, these changes are consistent with previously reported data at 12 h in this model of FHF (Arai et al., 2001; Shito et al., 2001), and show a biphasic trend with many of the measured parameters, suggesting a partial and temporary recovery around the 4–8 h time points. The partial recovery or lack of disease progression between the 1 and 4 h time points is consistent with the previous observations that a single injection of 1.4 g/kg D-galactosamine is non-lethal and that a second dose is required for lethality (Shito et al., 2001). Finally, there was no significant difference in the wet-to-dry weight ratio among the livers.

3.2. Metabolite production rates in perfused livers

To characterize the metabolic changes specific to liver during the progression of FHF, livers were isolated at different times after FHF, and perfused with a well-defined medium. The measured uptake/release rates of key metabolites as a function of time are shown in Fig. 1. During perfusion, control livers released glucose,

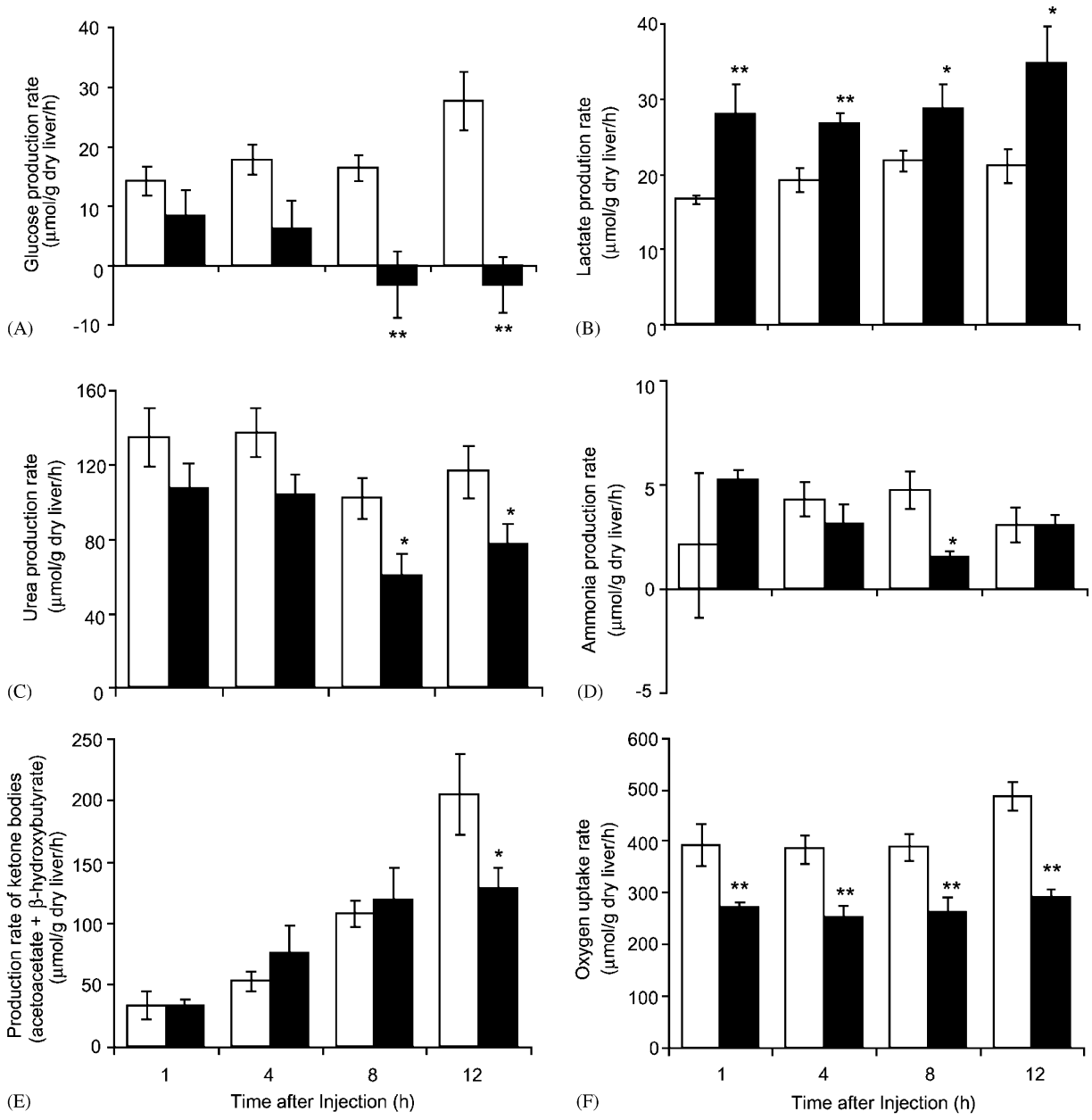

Fig. 1. Metabolite rate profiles by perfused livers after FHF induction. Production rates of glucose (A), lactate (B), urea (C), ammonia (D), and ketone bodies (E), and O_2 consumption rate (F) measured during perfusion of livers isolated from control (□) and FHF rats (■). The numbers of samples averaged per time point are indicated in Table 2. Data are represented as mean ± SE. Significant differences from the control group at each time point are indicated by *($P<0.05$) and **($P<0.01$).

consistent with fasting-induced gluconeogenesis. In FHF rat livers, glucose release switched to glucose uptake at the 8 and 12 h time points. Lactate was released from all livers; however, those from FHF rats produced significantly more lactate than controls at all time points examined. Unlike glucose production, lactate release did not vary over the experimental timeframe. Urea production by FHF rat livers significantly decreased at the 8 and 12 h time points. Nevertheless, a net release of ammonia was observed with all livers and there was no significant difference between control and FHF groups, except for a momentary decrease in FHF at 8 h. Ketone bodies (the sum of ACAC and BHBA) accumulated in the perfusates of all livers, which likely reflects fasting-induced ketogenesis. In the FHF group, ketone body production was significantly inhibited at 12 h, but not earlier. O_2 uptake rates did not significantly vary over time and were significantly lower in the FHF group at all times examined.

3.3. Amino acid metabolism in perfused livers

Fig. 2 shows the alterations in perfused liver uptake rates of the major amino acid groups induced by FHF over time and Table 2 shows the data for individual amino acids. In the FHF group, the uptake of gluconeogenic amino acids (aspartate, asparagine, serine, glycine, glutamate, glutamine, histidine, threonine, alanine, proline, methionine, lysine, cysteine, tyrosine, phenylalanine, arginine, valine, and isoleucine) decreased gradually to eventually lead to a net release at the 12 h time point. Control livers exhibited stable rates over this time period. In the FHF group, most gluconeogenic amino acids (serine, glycine, glutamate, glutamine, histidine, threonine, alanine, proline, methionine, lysine, tyrosine, phenylalanine, arginine, valine, and isoleucine) exhibited gradually decreasing rates that were significantly lower than controls. For some amino acids, this eventually led to a net release at the 12 h time point. Uptake of the urea cycle intermediates arginine and ornithine was not influenced by FHF. Considering the sum of BCAA, control livers released BCAA at stable rates for the first 8 h and then switched to a net uptake at 12 h. In the FHF group, BCAA were neither consumed nor released at 1 h, but a pronounced increase in release rate occurred in the time course leading to 12 h. The uptake of total AAA decreased gradually in both groups and a significant inhibition in the FHF group was observed at 12 h.

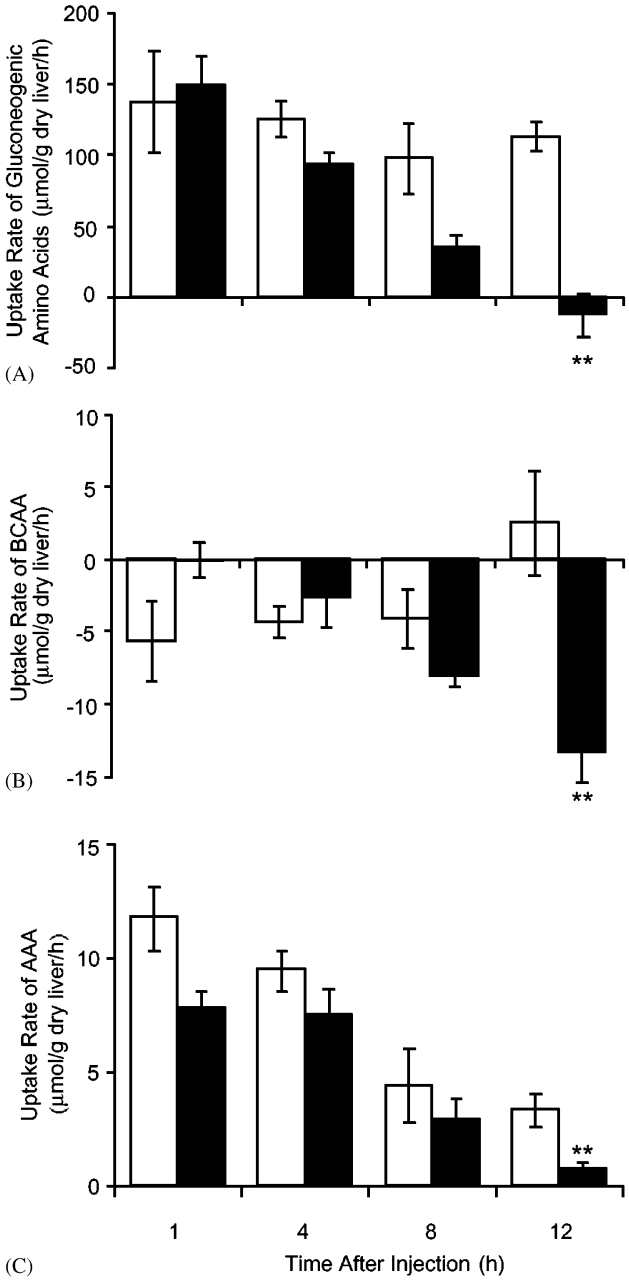

Fig. 2. Amino acid uptake rates by perfused livers. Uptake rates of gluconeogenic amino acids (A), BCAA (B), and AAA (C) measured during perfusion of livers from control (□) and FHF rats (■). A negative value indicates release from the liver. The numbers of samples per time point are indicated in Table 2. Data are represented as mean ± SE. Significant differences from the control group at each time point are indicated by **($P<0.01$).

3.4. Intrahepatic fluxes by mass balance analysis

From the measured rates of uptake and release of extrahepatic metabolites during the liver perfusions, intrahepatic fluxes were estimated with the gluconeogenic and glycolytic MFA models. The consistency index was used to determine which model resulted in the best fit of the data. For the control group, the gluconeogenic model always minimized the consistency index. For the FHF group, the 1 and 4 h data were best fit by the gluconeogenic model, and the 8 and 12 h data by the glycolytic model. The calculated intrahepatic fluxes are

Table 2
Uptake rate of individual amino acids by perfused livers[a]

	1 h		4 h		8 h		12 h	
	Control ($n=6$)	FHF ($n=5$)	Control ($n=9$)	FHF ($n=9$)	Control ($n=11$)	FHF ($n=7$)	Control ($n=6$)	FHF ($n=5$)
Aspartate (Asp)	0.5±0.4	0.2±0.2	0.3±0.1	0.4±0.2	0.3±0.2	0.1±0.2	0.4±0.2	−0.0±0.1
Glutamate (Glu)	−4.4±1.3	−2.8±0.1	−3.9±0.4	−3.3±0.6	−4.8±0.5	−5.5±0.6	−3.5±0.9	−6.9±1.1*
Serine (Ser)	6.0±2.9	6.8±1.1	5.7±0.8	5.5±1.0	6.6±2.0	4.2±0.6	7.5±1.6	0.0±1.7*
Asparagine (Asn)	10.0±2.9	11.8±1.9	8.2±1.1	8.5±1.4	8.4±2.2	5.3±0.9	8.4±1.3	4.2±0.9*
Glycine (Gly)	4.6±1.4	3.8±1.3	3.2±0.4	2.1±0.7	1.4±1.1	0.5±1.0	2.7±1.0	−0.6±0.9*
Glutamine (Gln)	70.8±20.9	68.0±18.3	65.1±10.3	33.1±6.1*	55.2±15.2	14.0±5.9	61.7±5.0	−3.8±11.6**
Histidine (His)	5.5±1.2	5.1±1.3	4.82±0.7	1.82±1.1*	2.1±0.7	−0.2±0.6*	1.9±1.0	−4.0±1.8*
Threonine (Thr)	0.5±1.6	1.6±1.7	0.4±0.7	−0.9±1.0	0.1±1.0	−2.3±0.5	2.4±1.3	−4.2±1.1*
Arginine (Arg)	16.5±5.1	26.5±1.3	16.2±2.2	25.0±3.6	17.5±3.2	11.1±1.3	11.7±1.9	14.4±3.0
Alanine (Ala)	9.8±2.4	9.6±1.1	8.5±0.7	8.4±0.6	7.1±1.8	6.9±1.2	7.0±0.7	2.9±0.4**
Proline (Pro)	4.8±0.9	4.2±0.4	3.6±0.5	2.6±0.6	2.0±1.0	2.0±0.8	3.0±0.9	−2.2±0.8**
Tyrosine (Tyr)	1.8±0.3	0.5±0.7	1.4±0.5	−0.7±0.8	0.1±0.7	−0.7±0.6	1.1±0.9	−2.0±0.2*
Cysteine (Cys)	−1.1±0.3	−0.7±0.2	−0.9±0.1	−1.0±0.1	−0.7±0.2	−0.5±0.1	−0.2±0.3	−1.0±0.3
Valine (Val)	−2.6±1.0	−1.3±0.3	−3.1±0.6	−1.3±0.9	−1.8±1.0	−3.5±0.5	0.5±1.2	−4.0±0.5*
Methionine (Met)	1.0±0.5	0.8±0.3	1.0±0.1	0.4±0.2*	0.8±0.3	0.2±0.2	0.8±0.4	−0.5±0.4*
Isoleucine (Ile)	0.5±1.4	3.6±1.1	2.6±0.5	1.7±1.1	1.6±1.1	−0.1±1.0	1.8±1.6	−3.6±1.0*
Ornithine (Orn)	−14.8±1.8	−12.9±1.7	−14.4±0.7	−14.8±2.2	−12.2±2.8	−8.8±1.9	−6.7±1.4	−8.3±0.9
Leucine (Leu)	−3.7±1.1	−2.3±0.3	−3.8±0.4	−3.1±0.9	−4.0±0.6	−4.5±0.7	−0.2±1.7	−5.8±0.9*
Lysine (Lys)	3.0±1.5	3.4±1.5	3.2±0.4	2.3±1.0	−0.4±1.1	0.0±1.2	3.4±1.5	−4.0±1.3*
Phenylalanine (Phe)	10.0±1.4	7.2±0.3	8.1±0.9	8.1±0.7	4.3±1.1	3.6±0.8	2.2±0.4	2.7±0.3

*$P<0.05$ compared with control. **$P<0.01$ compared with control.
[a]A negative value indicates net release. Data are presented as mean ± SE in μmol/g dry liver/h.

summarized in Fig. 3 (for complete data set, see Appendix). At the 1 h time point, TCA cycle fluxes (nos. 13–17) and portions of the gluconeogenic pathway (fluxes nos. 6, 7) were inhibited compared to controls, as indicated by the blue arrows, while lactate release increased (flux no. 11), as indicated by the red arrow. At the 4 h time point, urea cycle fluxes (nos. 19–20), several amino acid oxidation pathways (nos. 41, 43, 45, 46), aspartate synthesis from oxaloacetate (flux no. 48), and β-oxidation (flux no. 51) were downregulated, while the PPP (fluxes nos. 59–63) was activated. Urea cycle fluxes and aspartate synthesis remained depressed until the end of the experiment. At the 8 h time point, the PPP fluxes had returned to baseline; however, an early sign of gluconeogenesis switching to glycolysis was indicated by the reversal of flux no. 1, as shown by the orange arrow. At the 12 h time point, glycolysis was fully induced, amino acid entry into the TCA cycle was broadly inhibited, resulting in many amino acids being released, and ketogenesis was inhibited.

3.5. Principal component analysis

PCA was used to condense the large set of data into a small number of parameters (called principal components) that would provide a sensitive and intuitive way to track the evolution of FHF (see Fig. 4). Two principal components were calculated for the control and the FHF groups. Although a greater number of components could be used, two were found to be sufficient to account for over 90% of the variation in the data. Table 3 shows the parameters that have the highest weights (and thus the greatest impact) on each one of the principal components and in each experimental group. Using arterial plasma metabolite levels only, the PC1 coordinate was mainly comprised of the concentrations of glucose and lactate, while the PC2 coordinate involved the concentrations of lactate, glutamine, glucose, alanine, and ACAC. The corresponding scatter plot shows that PC1 clearly divides the control and FHF groups as early as the 1 h time point (Fig. 5A). There was no clear trend observed in PC2 until the 12 h time point, where a decrease was observed. This change in PC2 can be related to the increased lactate and glutamine plasma levels. The control group exhibited a downward shift along the PC1 axis in addition to PC2. Next, we determined the principal components using the measured extrahepatic liver perfusion data. The PC1 coordinate was mainly comprised of the O_2 consumption and CO_2 production rates, while the PC2 coordinate contained the BHBA, ACAC, glutamine, and urea rates. The corresponding scatter plot shows that PC1 clearly divided control and FHF groups even at the 1 h time point (Fig. 5B), and both groups exhibited an upward shift along the PC2 axis as a function of time. Overall, the ability to separate between control sham and FHF groups was not slightly better than with plasma data only; however, the evolution with time was

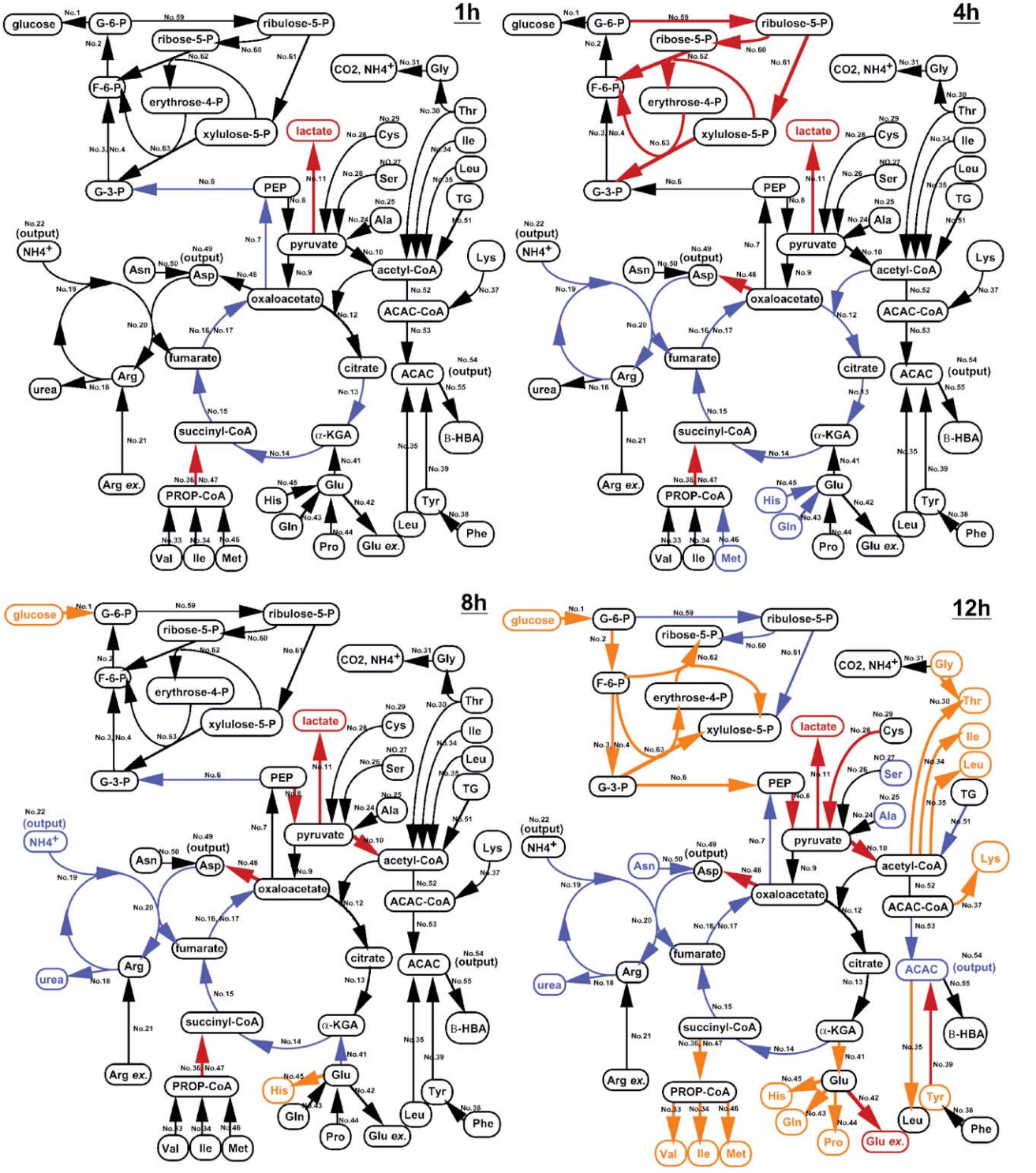

Fig. 3. Hepatic metabolic fluxes in perfused livers. Metabolic flux analysis was used to calculate intracellular pathway fluxes that account for the observed metabolite rate profiles and the stoichiometry of a simplified hepatic metabolic reaction network. For clarity, amino acid degradation pathways are grouped according to the points of entry into the TCA cycle, gluconeogenesis, and ketogenesis pathways. In addition, only selected fluxes are shown (the complete list is in Appendix). *Black arrows* indicate the direction of reaction assumed in the model. *Red arrows* indicate fluxes that are significantly higher than controls, *Blue arrows* show significantly inhibited fluxes, and *Orange arrows* show fluxes that reverse direction ($P<0.05$). G-6-P, glucose 6-phosphate; F-6-P, fructose 6-phosphate; G-3-P, glyceraldehyde 3-phosphate; PEP, phosphoenolpyruvate; TG, triacylglycerol; α-KGA, α-ketoglutarate; ACAC, acetoacetate; BHBA, β-hydroxybutyrate. Amino acids are abbreviated using the standard three-letter convention. Extrahepatic metabolites which are transported across the cell membrane and that feed into branch points of the network are denoted by the subscript *ex* to distinguish between intra- and extra-hepatic pools.

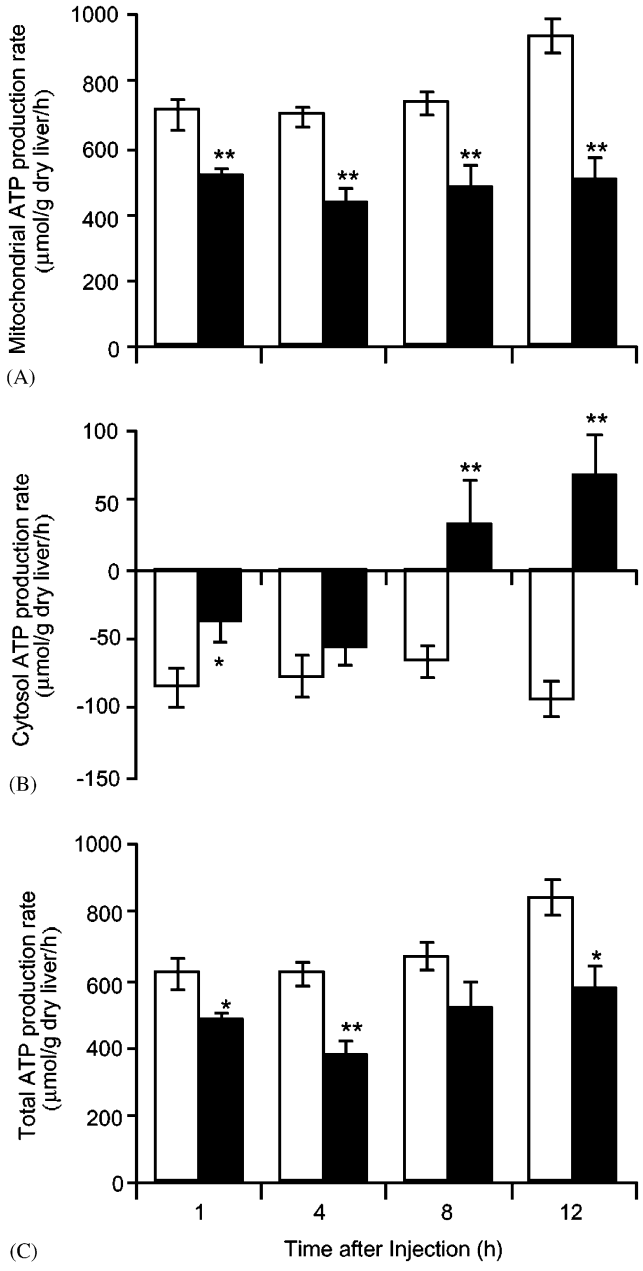

Fig. 4. Evolution of hepatic ATP production during FHF. ATP production rates of mitochondria, cytosol, and total (mitochondria + cytosol) were calculated from fluxes determined by MFA for control (□) and FHF rats (■), and are represented as mean ± SE. The numbers of samples per time point are indicated in Table 3. Significant differences from the control group at each time point are indicated by **($P<0.01$).

more clearly observed with perfusion data. Using the calculated intrahepatic fluxes, the first principal component PC1 was most heavily weighed by fluxes no. 56 (mitochondrial electron transport), no. 58 (O_2 uptake rate), and no. 57 (mitochondrial electron transport), while PC2 primarily consisted of fluxes no. 52 (ACAC-CoA production rate), no. 53 (ACAC production rate), and no. 57. The corresponding PC2 vs. PC1 scatter plot was very similar to that obtained with the measured extrahepatic fluxes (Fig. 5C).

4. Discussion

In this study, we characterized the evolution of the hepatic metabolic state in a D-galactosamine-induced FHF rat model by perfusing livers isolated up to 12 h after induction of FHF. The earliest metabolic change in liver was a decrease in gluconeogenesis eventually switching to glycolysis concomitant with inhibition of TCA cycle and electron transport fluxes, causing an increase in lactate release. Amino acid rates showed time-dependent alterations that were most apparent at 12 h, i.e. later than lactate, glucose or TCA cycle changes. These findings are consistent with prior reports suggesting that the injured liver acts as a major source of systemic lactate in the splanchnic circulation (Clemmesen et al., 2000) and that implicate the activation of glycolysis as a likely mechanism of increased hepatic lactate release (Clemmesen et al., 2000; Gore et al., 1996; James et al., 1999). Inhibition of pyruvate dehydrogenase has also been implicated (Vary et al., 1986), although in this study we observed an increase—rather than decrease—in the pyruvate dehydrogenase flux (no. 10). It is indeed likely that upregulating pyruvate dehydrogenase would likely draw more material from the pyruvate pool, and in turn consume more lactate, which is at equilibrium with pyruvate. Metabolic perturbations observed at the final 12 h time point were largely consistent with that previously reported in an earlier publication, including: (1) significantly decreased hepatic gluconeogenesis, (2) reduced amino acid entry into various points of the TCA cycle, (3) inhibition of intrahepatic aspartate synthesis leading to a reduction in urea cycle flux, and (4) compensatory increase in ammonia removal via glutamine synthesis from glutamate and a decrease in the conversion of glutamate to α-ketoglutarate (Arai et al., 2001).

Intracellular pathway fluxes were determined via metabolic flux analysis (MFA), which balances the major input and output metabolites according to well-known stoichiometric constraints defined by a metabolic model (Arai et al., 2001; Lee et al., 2000; Zupke and Stephanopoulos, 1995). To reduce complexity, only the pathways that handle the most substrate and significantly contribute to the overall carbon and nitrogen balances were included in the MFA model. Notably, we chose to ignore the contribution of protein degradation that occurred, as evidenced by the net release of specific branch-chain amino acids (Table 2) in all of the experimental groups, because the nature of the proteins that are degraded is unknown and the generated amino acids make up a relatively small proportion of the total amino acid flux into the liver. Furthermore, it was

Table 3
Classification of metabolites and intrahepatic fluxes according to their weights in principal components[a]

PC1		PC2	
Arterial plasma	*Arterial plasma*	*Arterial plasma*	*Arterial plasma*
Glucose	−0.967	Lactate	−0.891
Lactate	0.250	Glutamine	−0.354
Glutamine	0.057	Glucose	−0.254
ACAC	−0.017	Alanine	−0.068
BHBA	−0.012	ACAC	0.064
Measured uptake rates			
Oxygen	−0.843	BHBA	0.596
Carbon dioxide	−0.437	ACAC	0.450
BHBA	−0.173	Glutamine	−0.441
Glutamine	−0.155	Urea	−0.422
Urea	−0.151	Carbon dioxide	0.166
Intrahepatic fluxes[b]			
No. 56	−0.459	No. 52	0.385
No. 58	−0.423	No. 53	0.383
No. 57	−0.402	No. 57	0.341
No. 16	−0.260	No. 16	−0.266
No. 17	−0.258	No. 17	−0.256

[a]Negative values indicate that the parameter, when increasing, decreases the value of the principal component.
[b]Flux nos. refer to chemical reactions shown in Fig. 3 and the table in the Appendix.

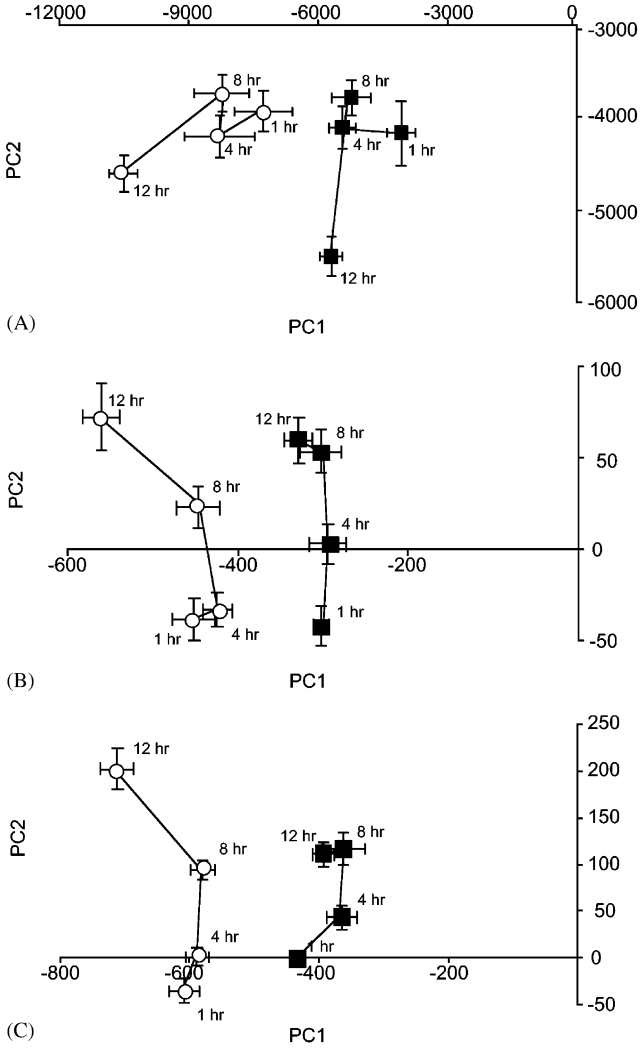

Fig. 5. Scatter plots of principal components based on arterial plasma metabolites, measured uptake/release rates of metabolites by perfused livers, and calculated intrahepatic fluxes. Principal component analysis was used to identify the five most sensitive parameters that can distinguish between control (○) and FHF (■) rat livers. Two principal components (PC1 and PC2) were determined using the following data sets: arterial plasma metabolite levels (A), measured metabolite uptake rates by perfused livers (B), and calculated intrahepatic fluxes (C). The definition of PC1 and PC2 for each data set is in Table 3, and the values are represented as mean ± SE. The numbers of samples per time point are indicated in Table 2.

necessary to create two slightly different models for gluconeogenic vs. glycolytic states in order to avoid futile cycling between pyruvate, oxaloacetate, and phosphoenolpyruvate. In the former case, we assumed that fluxes through pyruvate kinase and pyruvate dehydrogenase were negligible, while in the latter case, we assumed that pyruvate carboxylase was inhibited (Lee et al., 2000). We found better consistency between model and experimental data when the gluconeogenic model was fitted to data from the control group, which is expected in these fasted animals that are otherwise healthy. While FHF data from the 1 and 4 h time points were also better fitted by the gluconeogenic model, this was no longer the case afterwards, as the glycolytic model best fitted the 8 and 12 h data.

D-galactosamine treatment leads to the accumulation of UDP-galactosamine at the expense of UDP-galactose (Bauer et al., 1974). One published report indicates that D-galactosamine treatment induces glucose 6-phosphate dehydrogenase, the rate-limiting enzyme of the PPP (Watanabe et al., 1978). Since the PPP is a major source for de novo synthesis of nucleotides, as well as cytosolic NADPH, a co-factor in many biosynthetic reactions (Sabate et al., 1995), we added it to our MFA models, which were otherwise similar to that previously used to analyze metabolic data in D-galactosamine-induced FHF in rats (Arai et al., 2001). It is noteworthy that MFA calculations reveal that the measured rate of CO_2 strongly affects the PPP flux while it has very little impact on the rest of the MFA results. As pointed out in the Materials and Methods section, CO_2 measurements do not account for the possible increase in CO_2 levels in the form of HCO_3^- across the liver. Although this may underestimate the production of CO_2 and the calculated PPP, the changes observed are most likely to hold in a relative sense. Flux analysis indicated that the PPP was upregulated in the FHF group 4 h after the second D-galactosamine injection, and was subsequently inhibited. It is plausible that stimulation of the PPP is part of a tissue repair process with increased NADPH and nucleotide (for DNA synthesis) demand. PPP inhibition

at later times may be caused by damage from the second D-galactosamine dose. Further studies on this question could lead to a better understanding of the metabolic factors that eventually lead to recovery or death from FHF.

The results indicate that the TCA cycle and electron transport chain fluxes were inhibited by FHF, as reflected by the reduced O_2 consumption rate in perfused FHF rat livers. Recent reports indicate that D-galactosamine treatment damages mitochondria by promoting mitochondrial cytochrome c release from liver and cultured hepatocytes, as part of the induction of the apoptosis pathway (Kim et al., 2000; Quintero et al., 2002). On the other hand, this finding is in contrast with other studies that have reported that the hepatic O_2 uptake is elevated in liver failure patients and in an acute rat liver failure model induced by a single dose of D-galactosamine (1.1 g/kg) (Clemmesen et al., 1999; Makin et al., 1997). This discrepancy may be the result of a more severe disease as a result of a higher dose of D-galactosamine (two 1.4 g/kg injections) used to induce FHF in our study.

In the FHF group, a greater proportion of ATP was progressively derived from glycolysis (fluxes nos. 8–6) at the expense of mitochondrial oxidative phosphorylation (fluxes nos. 56 + 57) during the evolution of FHF, which occurred in parallel with a switch from gluconeogenesis to glycolysis. This is in striking contrast with the gluconeogenic and ketogenic states observed in the sham controls, which are the expected metabolic states in livers of fasted animals. In a prior study using a single D-galactosamine injection, TNF-α and IL-1β levels were significantly elevated (Shito et al., 2001) and both of these cytokines have been shown to inhibit gluconeogenesis in cultured rat hepatocytes (Ceppi and Titheradge, 1998; Christ and Nath, 1996). Thus, it is likely that cytokine-induced suppression is involved in our FHF group as well. The mechanism of induction of glycolysis in the FHF group is unclear, especially in a fasted state. The induction of glycolysis in FHF is nevertheless consistent with results of studies with humans undergoing acute liver failure suggesting that the injured liver acts as a major source of systemic lactate in the splanchnic circulation (Clemmesen et al., 2000), and that implicate the activation of glycolysis as a likely mechanism of increased hepatic lactate release (Clemmesen et al., 2000; Gore et al., 1996; James et al., 1999). Further studies, in particular focusing on the interaction of the glucagon, insulin, and cytokine signal transduction pathways, may shed light on the governing mechanisms.

The results of PCA of arterial plasma levels suggest that lactate is the most sensitive parameter that distinguishes between control and FHF rats (Table 3). Interestingly, blood lactate concentrations have been correlated with the probability of survival of acute liver failure patients (Bernal et al., 2002). Furthermore, PCA suggests that instead of lactate alone, a linear combination of glucose, lactate, and glutamine concentrations in arterial plasma could be used to more accurately separate the control and FHF groups. This lumped parameter is also more sensitive than the ketone body ratio and the Fischer ratio, which were significantly different from the controls at the 1 and 12 h time points only. The results of PCA of perfused liver data suggest that the metabolic state of liver in FHF is mainly characterized by the inhibition of mitochondrial electron transport, followed by the inhibition of ketogenesis. One prior study has indicated that plasma glucose and lactate levels reflect the inhibition of gluconeogenesis and activated glycolysis (James et al., 1999) Furthermore, other reports have suggested that glutamine uptake can drive mitochondrial ATP formation (Kovacevic and Morris, 1972; Piva and McEvoy-Bowe, 1998) and increased β-oxidation (Kim et al., 2002) such that the plasma concentration of glutamine may reflect changes in the oxidative phosphorylation pathway. Thus, the PCA analysis results with plasma are consistent in many ways with changes in perfused liver. Further study to establish the usefulness of PCA-derived parameters as a prognostic tool for FHF is warranted.

We conclude that in a lethal model of D-galactosamine-induced FHF, the earliest metabolic perturbations detected include an inhibition of TCA cycle fluxes and some parts of the gluconeogenic pathway, with a significant increase in lactate release. Furthermore, the data suggest that the main source of ATP production in the FHF liver gradually changes from mitochondrial oxidative phosphorylation to glycolysis. Taken together, these findings are consistent with the notion that D-galactosamine may cause early mitochondrial damage while cytosolic pathways for ATP synthesis remain functional. PCA analysis of the data suggest that a combination of glucose, lactate, and glutamine concentrations in arterial plasma may be a new avenue for the prognosis of FHF. Given that these results apply to D-galactosamine-induced in rats, further studies will be needed to generalize these findings to other causes of hepatic failure.

Acknowledgments

Supported in parts by the Shriners Hospitals for Children and the National Institutes of Health grants R01 GM58125 and R01 DK43371.

Appendix

See Table 4 for the reaction stoichiometry and fluxes calculated by metabolic flux analysis.

Table 4
Reaction stoichiometry and fluxes calculated by metabolic flux analysis[a]

Flux No.	Stoichiometry	Enzyme(s)	1 h		4 h		8 h		12 h	
			Control ($n = 6$)	FHF ($n = 5$)	Control ($n = 9$)	FHF ($n = 9$)	Control ($n = 11$)	FHF ($n = 7$)	Control ($n = 6$)	FHF ($n = 5$)
1	Glucose 6-phosphate → glucose + Pi	Glucose 6-phosphatase	14.2 ± 2.2	8.3 ± 4.5	17.8 ± 2.5	6.0 ± 5.0	16.3 ± 2.2	−3.3 ± 5.6**	27.7 ± 5.0	−3.3 ± 5.1**
2	Fructose 6-phosphate ↔ glucose 6-phosphate	Phosphohexose isomerase	23.3 ± 26.4	10.4 ± 4.1	21.9 ± 2.5	66.3 ± 23.1	72.3 ± 37.3	46.6 ± 51.7	153.2 ± 32.9	−3.2 ± 4.9**
3	Fructose 1,6-bisphosphate → fructose 6-phosphate + Pi	Fructose-1,6-bisphosphatase	35.0 ± 8.9	16.7 ± 5.4	33.8 ± 4.9	35.8 ± 7.8	43.0 ± 10.9	13.3 ± 19.0	73.5 ± 10.6	−2.9 ± 5.3**
4	2 glyceraldehyde 3-phosphate ↔ fructose 1,6-bisphosphate	Triose phosphate isomerase, fructose bisphosphatase, aldolase	40.0 ± 9.1	18.8 ± 6.4	37.8 ± 6.0	38.5 ± 7.8	45.2 ± 10.6	13.3 ± 19.0	74.6 ± 10.5	−2.7 ± 5.7**
5	glycerol + ATP + NAD^+ → glyceraldehyde 3−phosphate + ADP + NADH	Glycerol kinase, glycerol 3-phosphate dehydrogenase, triose phosphate isomerase	2.7 ± 1.0	3.9 ± 1.4	5.5 ± 1.6	5.2 ± 1.3	9.9 ± 0.9	9.0 ± 2.1	16.5 ± 2.1	9.1 ± 1.2*
6	Glyceraldehyde 3-phosphate + Pi + ADP + NAD^+ ↔ phosphoenolpyruvate + NADH + ATP	4 steps	84.9 ± 13.9	37.6 ± 16.0*	77.5 ± 15.4	57.5 ± 11.2	66.7 ± 11.3	1.1 ± 21.0*	93.3 ± 13.3	−14.3 ± 12.6**
7	Oxaloacetate + GTP ↔ phosphoenolpyruvate + GDP + CO_2	Phosphoenolpyruvate carboxykinase	87.7 ± 14.4	39.5 ± 16.4*	80.5 ± 15.7	59.1 ± 11.4	67.9 ± 11.5	34.5 ± 7.6	93.9 ± 13.7	31.1 ± 10.3**
8	Phosphoenolpyruvate + ADP ↔ pyruvate + ATP	Pyruvate kinase	0.0 ± 0.0	0.0 ± 0.0	0.0 ± 0.0	0.0 ± 0.0	0.0 ± 0.0	33.4 ± 24.0	0.0 ± 0.0	45.4 ± 18.3*
9	Pyruvate + CO_2 + ATP → oxaloacetate + ADP + Pi	Pyruvate carboxylase	9.2 ± 16.6	−19.0 ± 15.9	16.1 ± 11.0	5.9 ± 9.0	1.7 ± 13.1	0.0 ± 0.0	9.9 ± 0.3	0.0 ± 0.0
10	Pyruvate + NAD^+ → NADH + CO_2 + acetyl−CoA	Pyruvate dehydrogenase	0.0 ± 0.0	0.0 ± 0.0	0.0 ± 0.0	0.0 ± 0.0	0.0 ± 0.0	36.4 ± 29.7	0.0 ± 0.0	69.2 ± 17.6**
11	Pyruvate + NADH ↔ lactate + NAD^+	Lactate dehydrogenase	16.3 ± 0.5	27.9 ± 4.1*	19.2 ± 1.6	26.7 ± 1.5**	21.7 ± 1.4	28.8 ± 3.1*	20.6 ± 2.6	36.9 ± 7.9*
12	Oxaloacetate + acetyl−CoA → citrate	Citrate synthase	69.8 ± 14.0	32.7 ± 8.3	60.3 ± 8.6	19.7 ± 12.7*	46.2 ± 11.2	16.3 ± 14.5	23.1 ± 16.7	35.0 ± 11.9
13	Citrate + NAD^+ ↔ α-ketoglutarate + CO_2 + NADH	Aconitase, isocitrate dehydrogenase	65.7 ± 13.7	27.3 ± 8.1*	53.1 ± 7.5	17.5 ± 12.5*	44.4 ± 11.0	16.3 ± 14.5	22.2 ± 16.4	34.8 ± 11.1
14	α-ketoglutarate + CoA−SH + NAD^+ → succinyl-CoA + CO_2 + NADH	α-ketoglutarate dehydrogenase	141.2 ± 13.6	93.7 ± 8.8*	121.7 ± 7.3	55.2 ± 12.1**	100.6 ± 10.9	32.9 ± 14.4**	88.4 ± 15.9	35.1 ± 10.4*
15	Succinyl-CoA + Pi + GDP + FAD ↔ fumarate + CoA−SH + GTP + $FADH_2$	Succinyl-CoA synthetase, succinate dehydrogenase	131.9 ± 13.5	91.4 ± 9.2*	113.6 ± 7.3	51.5 ± 11.7**	97.5 ± 10.9	29.5 ± 14.4**	89.6 ± 15.3	26.8 ± 9.8**
16	Fumarate ↔ malate	Fumarase	256.3 ± 18.3	177.4 ± 16.9*	235.3 ± 14.8	137.6 ± 15.0**	185.5 ± 14.4	82.4 ± 18.8**	197.9 ± 18.9	92.3 ± 14.8**
17	Malate + NAD^+ ↔ oxaloacetate + NADH	Malate dehydrogenase	253.0 ± 17.9	174.1 ± 17.0*	230.6 ± 14.7	135.8 ± 14.6**	184.0 ± 14.2	82.4 ± 18.8**	197.1 ± 18.4	92.2 ± 14.3**
18	Arginine → urea + ornithine	Arginase	135.2 ± 14.7	107.1 ± 14.1	137.5 ± 13.1	103.8 ± 11.6	102.3 ± 11.1	60.3 ± 11.8*	116.5 ± 14.1	77.4 ± 13.8*
19	Ornithine + CO_2 + NH_4^+ + 2ATP ↔ citrulline + 2ADP + 2Pi	Cabamoyl phosphate synthetase, ornithine transcabamylase	114.8 ± 12.3	92.0 ± 11.6	115.3 ± 10.4	78.7 ± 9.3*	83.7 ± 9.3	44.3 ± 9.6*	103.6 ± 11.1	49.6 ± 11.2**
20	Citrulline + aspartate + ATP → arginine + fumarate + AMP + ppi	Argininosuccinate synthetase, argininosuccinase	113.9 ± 12.4	86.7 ± 11.7	113.8 ± 10.5	75.2 ± 9.4*	81.8 ± 9.3	43.5 ± 9.5*	101.9 ± 11.1	47.5 ± 11.2**

Table 4 (*continued*)

Flux No.	Stoichiometry	Enzyme(s)	1 h		4 h		8 h		12 h	
			Control ($n=6$)	FHF ($n=5$)	Control ($n=9$)	FHF ($n=9$)	Control ($n=11$)	FHF ($n=7$)	Control ($n=6$)	FHF ($n=5$)
21	Arginine uptake		16.5±4.7	26.5±1.6	16.2±2.2	25.0±3.6	17.5±3.2	11.1±1.3	11.7±1.9	14.4±3.0
22	NH_4^+ output		2.1±3.2	5.2±0.5	4.3±0.8	3.1±1.0	4.7±0.9	1.5±0.3*	2.7±0.8	2.8±0.6
23	Ornithine output		14.8±1.6	12.9±1.7	14.4±0.7	14.8±2.2	12.2±2.8	8.8±1.9	6.7±1.4	8.3±0.9
24	Alanine + NAD^+ → pyruvate + NH_4^+ + NADH	Alanine aminotransferase, glutamate dehydrogenase	12.9±5.2	7.7±4.6	15.4±3.3	14.2±2.7	10.8±4.1	13.3±2.9	11.1±3.1	20.5±3.7
25	Alanine uptake		9.8±2.2	9.6±1.1	8.5±0.7	8.4±0.6	7.1±1.8	6.9±1.2	7.0±0.7	2.9±0.4**
26	Serine → NH_4^+ + pyruvate	Serine dehydratase	12.4±7.6	4.9±6.9	15.8±5.0	14.6±4.1	10.2±5.9	12.4±4.1	15.4±4.7	24.3±5.7
27	Serine uptake		6.0±2.6	6.8±1.1	5.7±0.8	5.5±1.0	4.7±1.9	3.9±0.6	7.5±1.6	0.0±1.7**
28	Cysteine + NAD^+ SO_3^{2-} → pyruvate + thiosulfate + NH_4^+ + NADH	Cysteine transaminase, 3-mercaptopyruvate sulfurtransferase	3.0±4.9	−1.8±4.5	7.0±3.3	5.3±2.7	3.7±3.8	6.1±2.7	4.6±3.0	16.0±3.8*
29	Cysteine uptake		−1.2±0.3	−0.7±0.2	−0.9±0.1	−1.0±0.1	−0.7±0.2	−0.5±0.1	−0.2±0.3	−1.0±0.3
30	Threonine + CoA−SH + NAD^+ → glycine + acetyl−CoA + NADH	Serine hydroxymethyl transferase	0.5±1.5	1.6±1.7	0.4±0.7	−0.9±1.0	0.1±1.0	−2.3±0.5	2.4±1.3	−4.2±1.1**
31	2glycine + NAD^+ → serine + NADH + CO_2 + NH_4^+	Glycine synthase	4.5±2.6	1.5±2.5	5.1±1.8	3.8±1.5	2.7±2.0	2.3±1.4	4.7±1.7	6.3±2.0
32	Glycine uptake		4.6±1.3	3.8±1.3	3.2±0.4	2.1±0.7	1.4±1.1	0.5±0.9	2.7±1.0	−0.6±0.9*
33	Valine + α-ketoglutarate + 2NAD^+ + FAD + ATP + CoA−SH → glutamate + (S)methylmalonyl−CoA + 2NADH + $FADH_2$ + CO_2 + 2Pi	8 steps	−2.6±0.9	−1.3±0.3	−3.1±0.6	−1.3±0.9	−1.8±1.0	−3.5±0.5	0.5±1.2	−4.0±0.5**
34	Isoleucine + α-ketoglutarate + 2NAD^+ + FAD + ATP + 2CoA−SH → glutamate + (S)methylmalonyl−CoA + acetyl−CoA + 2NADH + $FADH_2$ + ADP + Pi	7 steps	0.5±1.2	3.6±1.1	2.6±0.5	1.7±1.1	1.6±1.1	−1.1±0.9	1.8±1.6	−3.6±1.0*
35	Leucine + α-ketoglutarate + NAD^+ + FAD + ADP + Pi → glutamate + NADH + $FADH_2$ + ATP + acetoacetate + acetyl-CoA	6 steps	−3.7±1.0	−2.3±0.3	−3.8±0.4	−3.1±0.9	−4.0±0.6	−4.5±0.7	−0.2±1.7	−5.8±0.9*
36	(S)methylmalonyl-CoA → succinyl−CoA	Methylmalonyl-CoA epimerase and methylmalonyl-CoA mutase	−6.2±1.9	0.2±1.6*	−4.4±1.3	−2.0±1.7	−1.7±1.8	−3.4±1.0	1.8±2.3	−8.2±1.6**
37	Lysine + 2α-ketoglutarate + 3NAD^+ + CoA−SH + FAD → 2glutamate + 3NADH + 2CO_2 + $FADH_2$ + acetoacetyl−CoA	7 steps	3.0±1.4	3.4±1.5		3.2±0.4	2.3±1.0	−0.4±1.1	0.0±1.2	3.4±1.5
38	Phenylalanine + H_4biopterin + O_2 → H_2biopterin + tyrosine	Phenylalanine hydroxylase	10.0±1.3	7.2±0.3	8.1±0.9	8.1±0.7	4.3±1.1	3.6±0.8	2.2±0.4	2.7±0.3
39	Tyrosine + α-ketoglutarate + $2O_2$ → glutamate + CO_2 + fumarate + acetoacetate	5 steps	13.8±4.8	2.6±4.8	12.6±3.7	12.7±2.7	7.6±3.8	9.3±2.8	7.2±3.0	18.1±3.4*
40	Tyrosine uptake		1.8±0.3	0.5±0.7	1.4±0.5	−0.7±0.8	0.1±0.7	−0.7±0.6	1.1±0.9	−2.0±0.2*
41	Glutamate + NAD^+ ↔ α-ketoglutarate + NADH + NH_4^+	Glutamate dehydrogenase	93.1±13.3	79.7±12.8	88.8±8.5	54.2±6.3**	60.4±10.5	17.8±6.4*	82.9±7.0	−2.8±9.2**
42	Glutamate output		4.4±1.2	2.8±0.1	3.9±0.4	3.3±0.6	4.8±0.5	5.5±0.6	3.5±0.9	6.9±1.1*
43	Glutamine → glutamate + NH_4^+	Glutaminase	70.8±19.1	68.0±18.3	65.1±10.3	33.1±6.1**	55.2±15.2	14.0±5.9	61.7±5.0	−3.8±11.6**
44	Proline + $0.5O_2$ + NAP^+ → glutamate + NADH	Proline oxidase, 1-pyrroline 5-carboxylate dehydrogenase	4.8±0.8	4.2±0.4	3.6±0.5	2.6±0.6	2.0±1.0	2.0±0.8	3.0±0.9	−2.2±0.8**
45	Histidine + H_4folate → NH_4^+ + N^5−formiminoH_4folate + glutamate	4 steps	5.5±1.1	5.1±1.3	4.8±0.7	1.8±1.2*	2.1±0.7	−0.2±0.6*	1.9±1.0	−4.0±1.8*
46	Methionine + 2ATP + serine + NAD^+ + CoA−SH → PPi + Pi + ADP + AMP + adenosine + cysteine + NADH + CO_2 + propionyl−CoA	6 steps	1.0±0.5	0.8±0.3	1.0±0.1	0.4±0.2*	0.8±0.3	0.2±0.2	0.8±0.3	−0.5±0.4*
47	Propionyl−CoA + ATP + CO_2 → (S)methylmalonyl−CoA + ADP + Pi	Propionyl-CoA carboxylase	−1.2±0.6	0.5±1.0	−0.1±1.0	−0.8±0.5	−0.2±0.5	0.2±0.2	0.3±0.6	−0.5±0.5

48	Oxaloacetate + NH_4^+ + NADH ↔ aspartate + NAD^+	Aspartate aminotransferase, glumamate dehydrogenase	101.1 ± 12.0	78.9 ± 11.2	100.3 ± 8.8	60.9 ± 7.6**	69.8 ± 9.2	31.6 ± 7.5*	89.1 ± 8.8	25.9 ± 9.7**
49	Aspartate output		0.5 ± 0.4	0.2 ± 0.2	0.3 ± 0.1	0.4 ± 0.2	0.3 ± 0.2	0.1 ± 0.2	0.4 ± 0.2	0.0 ± 0.1
50	Asparagine → aspartate + NH_4^+	Asparaginase	10.1 ± 2.7	11.8 ± 1.9	8.9 ± 1.1	8.5 ± 1.4	8.4 ± 2.2	5.3 ± 0.9	8.4 ± 1.3	4.2 ± 0.9*
51	Triacylglycerol + 3ATP + 24CoA-SH + 21FAD + 21NAD^+ → glycerol + 24acetyl−CoA + 21$FADH_2$ + 21NADH + 3AMP + 6Pi	β-oxidation	4.9 ± 0.8	4.2 ± 0.6	6.6 ± 0.8	6.4 ± 1.1	10.8 ± 0.7	9.0 ± 2.1	17.0 ± 1.9	9.1 ± 1.1**
52	2acetyl-CoA ↔ acetoacetyl−CoA + CoA−SH	Thiolase	22.3 ± 10.4	34.9 ± 7.6	47.8 ± 9.4	65.4 ± 16.9	105.7 ± 10.0	114.4 ± 19.9	194.6 ± 29.4	119.5 ± 16.1
53	Acetoacetyl−CoA → acetoacetate + CoA−SH	Acetoacetyl-CoA hydrolase	24.4 ± 10.4	35.6 ± 7.2	47.9 ± 9.3	67.3 ± 17.0	104.8 ± 10.0	114.4 ± 19.9	197.7 ± 29.4	115.4 ± 16.4*
54	Acetoacetate output		20.6 ± 8.9	13.8 ± 1.3	17.0 ± 4.2	36.5 ± 8.3	40.6 ± 7.0	57.6 ± 14.5	85.3 ± 11.5	52.4 ± 5.9*
55	Acetoacetate + NADH ↔ β-hydroxybutyrate + NAD^+	β-hydroxybutyrate dehydrogenase	13.1 ± 2.8	19.3 ± 5.4	36.4 ± 8.4	39.8 ± 14.6	67.5 ± 6.2	61.6 ± 13.3	119.1 ± 27.1	75.3 ± 15.5
56	NADH + 0.5O_2 → NAD	Mitochondrial electron transport chain	471.5 ± 40.4	330.4 ± 13.6*	443.0 ± 27.9	247.2 ± 38.6**	415.5 ± 31.2	270.2 ± 56.7*	483.4 ± 41.8	307.9 ± 21.5**
57	$FADH_2$ + 0.5O_2 → FAD	Mitochondrial electron transport chain	232.3 ± 21.9	183.8 ± 12.8	251.8 ± 17.9	185.3 ± 22.8*	320.6 ± 17.7	210.0 ± 37.9*	452.4 ± 30.8	200.6 ± 25.1**
58	O_2 uptake		392.5 ± 28.2	273.2 ± 6.8**	384.2 ± 19.1	251.5 ± 25.7**	388.9 ± 21.3	263.4 ± 28.5**	486.2 ± 23.2	292.0 ± 17.8**
59	Glucose 6-P + 2$NADP^+$ → ribulose 5-P + 2NADPH	Glucose 6-P DH, 6-Pgluconolactonase, and P-gluconate DH	4.1 ± 26.6	0.0 ± 0.0	0.0 ± 0.0	57.5 ± 23.6*	53.7 ± 37.9	49.9 ± 49.8	124.4 ± 33.4	0.0 ± 0.0**
60	Ribulose 5-P ↔ ribose 5-P	Ribose 5-P pentose isomerase	2.5 ± 8.8	0.5 ± 0.3	0.9 ± 0.3	19.8 ± 7.8*	18.4 ± 12.5	16.6 ± 16.6	41.7 ± 11.1	0.0 ± 0.2**
61	Ribulose 5-P ↔ xylulose 5-P	Ribulose-P 3-epimerase	−2.6 ± 18.0	−2.3 ± 1.5	−4.3 ± 1.3	35.5 ± 15.9*	33.4 ± 25.9	33.2 ± 33.2	81.7 ± 22.6	−0.1 ± 1.0**
62	Ribose 5-P + xylulose 5-P ↔ erythrose 5-P + fructose 6-P	Transketolase and transaldolase	−1.7 ± 9.0	−1.3 ± 0.8	−2.5 ± 0.8	17.5 ± 8.0*	16.5 ± 13.0	16.6 ± 16.6	40.8 ± 11.3	−0.1 ± 0.6**
63	Erythrose 4-P + xylulose 5-P ↔ fructose 6-P + glyceraldehyde 3-P	Transketolase	−5.0 ± 9.3	−2.8 ± 1.8	−5.2 ± 1.6	15.7 ± 8.1*	15.0 ± 13.4	16.6 ± 16.6	40.0 ± 11.6	−0.2 ± 1.2**
64	CO_2 production		197.8 ± 18.5	95.0 ± 15.4**	143.4 ± 15.8	125.2 ± 7.8	189.5 ± 38.3	133.8 ± 9.4	234.9 ± 16.6	133.1 ± 14.0**

*$P<0.05$, **$P<0.01$ compared to control at same time point; Abbreviations: ADP, adenosine diphosphate; AMP, adenosine monophosphate; GDP, guanosine diphosphate; GTP, guanosine triphosphate

[a]Data shown are mean (∝mol/g dry liver/h) ± SE. A negative value indicates that the net flux is in the opposite direction of that shown in the "Stoichiometry" column.

References

Arai, K., Lee, K., Berthiaume, F., Tompkins, R.G., Yarmush, M.L., 2001. Intrahepatic amino acid and glucose metabolism in a D-galactosamine-induced rat liver failure model. Hepatology 34, 360–371.

Ascher, N.L., Lake, J.R., Emond, J.C., Roberts, J.P., 1993. Liver transplantation for fulminant hepatic failure. Arch. Surg. 128, 677–682.

Bauer, C.H., Lukaschek, R., Reutter, W.G., 1974. Studies on the golgi apparatus. Cumulative inhibition of protein and glycoprotein secretion by D-galactosamine. Biochem. J. 142, 221–230.

Bernal, W., Donaldson, N., Wyncoll, D., Wendon, J., 2002. Blood lactate as an early predictor of outcome in paracetamol-induced acute liver failure: a cohort study. Lancet 359, 558–563.

Bihari, D., Gimson, A.E., Lindridge, J., Williams, R., 1985. Lactic acidosis in fulminant hepatic failure. Some aspects of pathogenesis and prognosis. J. Hepatol., 405–416.

Bismuth, H., Samuel, D., Gugenheim, J., Castaing, D., Bernuau, J., Rueff, B., Benhamou, J.P., 1987. Emergency liver transplantation for fulminant hepatitis. Ann. Intern. Med. 107, 337–341.

Ceppi, E.D., Titheradge, M.A., 1998. The importance of nitric oxide in the cytokine-induced inhibition of glucose formation by cultured hepatocytes incubated with insulin, dexamethasone, and glucagon. Arch. Biochem. Biophys. 349, 167–174.

Christ, B., Nath, A., 1996. Impairment by interleukin 1 beta and tumour necrosis factor alpha of the glucagon-induced increase in phosphoenolpyruvate carboxykinase gene expression and gluconeogenesis in cultured rat hepatocytes. Biochem. J. 320, 161–166 (Erratum in: Biochem. J. 321, 903, 1997).

Clemmesen, J.O., Gerbes, A.L., Gulberg, V., Hansen, B.A., Larsen, F.S., Skak, C., Tygstrup, N., Ott, P., 1999. Hepatic blood flow and splanchnic oxygen consumption in patients with liver failure. Effect of high-volume plasmapheresis. Hepatology 29, 347–355.

Clemmesen, J.O., Hoy, C.E., Kondrup, J., Ott, P., 2000. Splanchnic metabolism of fuel substrates in acute liver failure. J. Hepatol. 33, 941–948.

Cohen, S.A., De Antonis, K.M., 1994. Applications of amino acid derivatization with 6-aminoquinolyl-N-hydroxysuccinimidyl carbamate. Analysis of feed grains, intravenous solutions and glycoproteins. J. Chromatogr. A 661, 25–34.

Devictor, D., Desplanques, L., Debray, D., Ozier, Y., Dubousset, A.M., Valayer, J., Houssin, D., Bernard, O., Huault, G., 1992. Emergency liver transplantation for fulminant liver failure in infants and children. Hepatology 16, 1156–1162.

Fischer, J.E., Rosen, H.M., Ebeid, A.M., James, J.H., Keane, J.M., Soeters, P.B., 1976. The effect of normalization of plasma amino acids on hepatic encephalopathy in man. Surgery 80, 77–91.

Gore, D.C., Jahoor, F., Hibbert, J.M., DeMaria, E.J., 1996. Lactic acidosis during sepsis is related to increased pyruvate production, not deficits in tissue oxygen availability. Ann. Surg. 224, 97–102.

James, J.H., Luchette, F.A., McCarter, F.D., Fischer, J.E., 1999. Lactate is an unreliable indicator of tissue hypoxia in injury or sepsis. Lancet 354, 505–508.

Kim, Y.M., Kim, T.H., Chung, H.T., Talanian, R.V., Yin, X.M., Billar, T.R., 2000. Nitric oxide prevents tumor necrosis factor alpha-induced rat hepatocyte apoptosis by the interruption of mitochondrial apoptotic signaling through S-nitrosylation of caspase-8. Hepatology 32, 770–778.

Kim, S.C., Pierro, A., Zamparelli, M., Spitz, L., Eaton, S., 2002. Fatty acid oxidation in neonatal hepatocytes: effects of sepsis and glutamine. Nutrition 18, 298–300.

Kovacevic, Z., Morris, H.P., 1972. The roll of glutamine in the oxidative metabolism of malignant cells. Cancer Res. 32, 326–333.

Lee, W.M., 1993. Acute liver failure. N. Engl. J. Med. 329, 1862–1872.

Lee, K., Berthiaume, F., Stephanopoulos, G.N., Yarmush, D.M., Yarmush, M.L., 2000. Metabolic flux analysis of postburn hepatic hypermetabolism. Metab. Eng. 2, 312–327.

Makin, A.J., Hughes, R.D., Williams, R., 1997. Systemic and hepatic hemodynamic changes in acute liver injury. Am. J. Physiol. 272 (Gastrointest. Liver Physiol. 3), G617–G625.

Mizock, B.A., 1999. Nutritional support in hepatic encephalopathy. Nutrition 15, 220–228.

Mortimore, G.E., Surmacz, C.A., 1984. Liver perfusion: an in vitro technique for the study of intracellular protein turnover and its regulation in vivo. Proc. Nutr. Soc. 43, 161–177.

Ozawa, K., Kamiyama, Y., Kimura, K., Yamamoto, M., Aoyama, H., Yasuda, K., Tobe, T., 1983. Contribution of the arterial blood ketone body ratio to elevate plasma amino acids in hepatic encephalopathy of surgical patients. Am. J. Surg. 146, 299–305.

Ozawa, K., Chance, B., Tanaka, A., Iwata, S., Kitai, T., Ikai, I., 1992. Linear correlation between acetoacetate/beta-hydroxybutyrate in arterial blood and oxidized flavoprotein/reduced pyridine nucleotide in freeze-trapped human liver tissue. Biochim. Biophys. Acta 1138, 350–352.

Piva, T.J., McEvoy-Bowe, E., 1998. Oxidation of glutamine in HeLa cells: role and control of truncated TCA cycles in tumour mitochondria. J. Cell Biochem. 68, 213–225.

Quintero, A., Pedraza, C.A., Pedraza, C.A., Siendones, E., Kamal ElSaid, A.M., Colell, A., Garcia-Ruiz, C., Montero, J.L., De la Mata, M., Fernandez-Checa, J.C., Mino, G., Muntane, J., 2002. PGE1 protection against apoptosis induced by D-galactosamine is not related to the modulation of intracellular free radical production in primary culture of rat hepatocytes. Free Radic. Res. 36, 345–355.

Record, C.O., Iles, R.A., Cohen, R.D., Williams, R., 1975. Acid-base and metabolic disturbances in fulminant hepatic failure. Gut, 144–149.

Record, C.O., Buxton, B., Chase, R.A., Curzon, G., Murray-Lyon, I.M., Williams, R., 1976. Plasma and brain amino acids in fulminant hepatic failure and their relationship to hepatic encephalopathy. Eur. J. Clin. Invest. 6, 387–394.

Rosen, H.M., Yoshimura, N., Hodgman, J.M., Fischer, J.E., 1977. Plasma amino acid patterns in hepatic encephalopathy of differing etiology. Gastroenterology 72, 483–487.

Roth, E., Steininger, R., Winkler, S., Langle, F., Grunberger, T., Fugger, R., Muhlbacher, F.L., 1994. Arginine deficiency after liver transplantation as an effect of arginase efflux from the graft. Influence on nitric oxide metabolism. Transplantation 57, 665–669.

Sabate, L., Franco, R., Canela, E.I., Centelles, J.J., Cascante, M., 1995. A model of the pentose phosphate pathway in rat liver cells. Mol. Cell. Biochem. 142, 9–17.

Saibara, T., Onishi, S., Sone, J., Yamamoto, N., Shimahara, Y., Mori, K., Ozawa, K., Yamamoto, Y., 1991. Arterial ketone body ratio as a possible indicator for liver transplantation in fulminant hepatic failure. Transplantation 51, 782–786.

Saibara, T., Maeda, T., Onishi, S., Yamamoto, Y., 1994. Plasma exchange and the arterial blood ketone body ratio in patients with acute hepatic failure. J. Hepatol. 20, 617–622.

Shito, M., Balis, U.J., Tompkins, R.G., Yarmush, M.L., Toner, M., 2001. A fulminant hepatic failure model in the rat: involvement of interleukin-1beta and tumor necrosis factor-alpha. Dig. Dis. Sci. 46, 1700–1708.

Skoal, R.R., Rohlf, F.J., 1969. Biometry. The Principles and Practice of Statistics in Biological Research. WH Freeman, San Francisco, CA.

Vary, T.C., Siegel, J.H., Nakatani, T., Sato, T., Aoyama, H., 1986. Effect of sepsis on activity of pyruvate dehydrogenase complex in skeletal muscle and liver. Am. J. Physiol. 250 (Endocrinology. Metabolism 6), E634–E640.

Watanabe, A., Akamatsu, K., Takesue, A., Taketa, K., 1978. Dysregulation of protein synthesis in injured liver. A comparative study on microsomal and cytosole enzyme activities, microsomal lipoperoxidation and polysomal pattern in D-galactosamine and carbon tetrachloride-injured livers. Enzyme 23, 320–327.

Yamaguchi, Y., Yu, Y.M., Zupke, C., Yarmush, D.M., Berthiaume, F., Tompkins, R.G., Yarmush, M.L., 1997. Effect of burn injury on glucose and nitrogen metabolism in the liver: preliminary studies in a perfused liver system. Surgery 121, 295–303.

Zimmermann, C., Ferenci, P., Pifl, C., Yurdaydin, C., Ebner, J., Lassmann, H., Roth, E., Hortnagl, H., 1989. Hepatic encephalopathy in thioacetamide-induced acute liver failure in rats: characterization of an improved model and study of amino acidergic neurotransmission. Hepatology 9, 594–601.

Zupke, C.A., Stephanopoulos, G., 1995. Intracellular flux analysis in hybridomas using mass balance and in vitro ^{13}C NMR. Biotechnol. Bioeng. 45, 292–303.

Zupke, C.A., Stefanovich, P., Berthiaume, F., Yarmush, M.L., 1998. Metabolic effects of stress mediators on cultured hepatocytes. Biotechnol. Bioeng. 58, 222–230.